J|A|C|S
ARTICLES
Published on Web 06/05/2004

How Delocalized Is *N,N,N′,N′*-Tetraphenylphenylenediamine Radical Cation? An Experimental and Theoretical Study on the Electronic and Molecular Structure

Adriana V. Szeghalmi,[†] Marco Erdmann,[†] Volker Engel,[†] Michael Schmitt,*[,†] Stephan Amthor,[‡] Volker Kriegisch,[‡] Gilbert Nöll,[‡] Rainer Stahl,[‡] Christoph Lambert,*[,‡] Dirk Leusser,[§] Dietmar Stalke,[§] Manfred Zabel,[⊥] and Jürgen Popp[||]

Contribution from the Institut für Physikalische Chemie, Julius-Maximilians-Universität Würzburg, Am Hubland, D-97074 Würzburg, Germany, Institut für Organische Chemie, Julius-Maximilians-Universität Würzburg, Am Hubland, D-97074 Würzburg, Germany, Institut für Anorganische Chemie, Julius-Maximilians-Universität Würzburg, Am Hubland, D-97074 Würzburg, Germany, Naturwissenschaftliche Fakultät IV, Chemie und Pharmazie, Zentrale Analytik, Universität Regensburg, D-93040 Regensburg, Germany, and Institut für Physikalische Chemie, Friedrich Schiller-Universität Jena, D-07743 Jena, Germany

Received November 11, 2003; E-mail: mschmitt@phys-chemie.uni-wuerzburg.de

Abstract: The electronic and molecular structure of *N,N,N′,N′*-tetraphenylphenylenediamine radical cation **1**$^+$ is in focus of this study. Resonance Raman experiments showed that at least eight vibrational modes are strongly coupled to the optical charge resonance band which is seen in the NIR. With the help of a DFT-based vibrational analysis, these eight modes were assigned to symmetric vibrations. The contribution of these symmetric modes to the total vibrational reorganization energy is dominant. These findings are in agreement with the conclusions from a simple two-state two-mode Marcus−Hush analysis which yields a tiny electron-transfer barrier. The excellent agreement of the X-ray crystal structure analysis and the DFT computed molecular structure of **1**$^+$ on one hand as well as the solvent and solid-state IR spectra and the DFT-calculated IR active vibrations on the other hand prove **1**$^+$ adopts a symmetrical delocalized Robin−Day class III structure both in the solid state and in solution.

Introduction

Mixed-valence (MV) species play a dominant role as simple model systems in the investigation of adiabatic electron transfer (ET) processes.[1−6] The usually employed one-dimensional MV systems consist of two redox centers (ligand coordinate metals or organic redox active moieties) that are connected via a bridge molecule. If the two redox centers have a different oxidation state, an electron or a hole can be transferred either by optical excitation or thermally. Several structural parameters which control the electron (hole) transfer rate were varied and investigated such as the type of the redox centers (purely organic vs ligand complexed metal ions), the bridge length, the nature of the bridge (conjugate vs nonconjugate), the local bridge energy, etc. The electronic coupling V of two diabatic (i.e., noninteracting) states in which the excess electron (or hole) is localized on the left-hand or right-hand redox center describes the communication between these centers.

According to Robin and Day,[7] MV species can be classified into three categories: class I with practically no coupling between the different redox states, class II with intermediate coupling, and class III in which the excess electron (or hole) is delocalized over the two redox centers. The adiabatic potential energy surface (PES) for the one-dimensional degenerate case can be constructed by coupling two diabatic states which are represented by quadratic potentials in a 2×2 matrix (see Figure 1 and section B) where V is the electronic coupling and λ the reorganization energy of the diabatic potentials. The optical excitation from one energy minimum of the ground state surface to the excited state yields directly λ as long as $2V < \lambda$.[8,9] The absorption band associated with this optical excitation is usually found in the NIR and is called intervalence charge-transfer band (IV-CT) in the case of class II and charge resonance band in

[†] Institut für Physikalische Chemie.
[‡] Institut für Organische Chemie.
[§] Institut für Anorganische Chemie.
[⊥] Universität Regensburg.
[||] Friedrich Schiller-Universität Jena.

(1) Crutchley, R. J. *Adv. Inorg. Chem.* **1994**, *41*, 273−325.
(2) Creutz, C. *Progr. Inorg. Chem.* **1983**, *30*, 1−73.
(3) Sutin, N. *Progr. Inorg. Chem.* **1983**, *30*, 441−498.
(4) Launay, J.-P. *Chem. Soc. Rev.* **2001**, *30*, 386-397.
(5) Barbara, P. F.; Meyer, T. J.; Ratner, M. A. *J. Phys. Chem.* **1996**, *100*, 13148−13168.
(6) Nelsen, S. F.; Ismagilov, R. F.; Trieber, D. A. *Science* **1997**, *278*, 846−849.
(7) Robin, M. B.; Day, P. *Adv. Inorg. Chem. Radiochem.* **1967**, *10*, 247−422.
(8) Wong, K. Y.; Schatz, P. N. *Progr. Inorg. Chem.* **1981**, *28*, 369−449.
(9) Brunschwig, B. S.; Creutz, C.; Sutin, N. *Chem. Soc. Rev.* **2002**, *31*, 168−184.

10.1021/ja0395386 CCC: $27.50

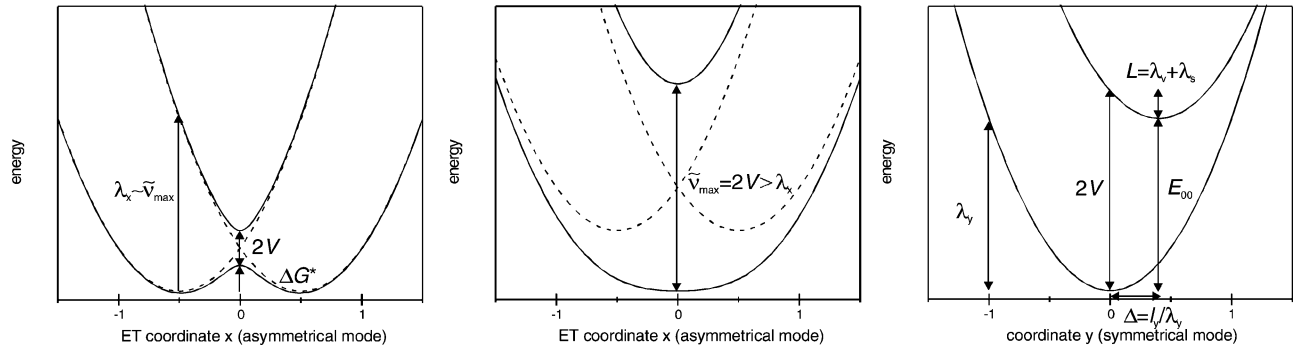

Figure 1. Diabatic potentials (dashed lines) and adiabatic potentials (solid lines) for a class II system (left diagram), a class III system (center diagram) along the asymmetrical *x* mode, and the corresponding section along the symmetrical *y* mode at $x = 0$ (right diagram) as derived from the solutions of eq 1. λ_v and λ_s refer to the vibrational and solvent reorganization energies as derived from the resonance Raman analysis, see below.

the case of class III.[10] While for MV species of class I or II there exists a barrier ΔG^* for the thermal ET, this barrier vanishes for class III compounds at $2V > \lambda$. If one seeks to use MV species as electronic switching or storage units for future optoelectronic devices on a molecular level, it is of utmost importance to assess the degree of delocalization in these MV species.[11] Thus, in particular the transition between class II and class III has attracted considerable interest in recent years.[9,12−21]

While for many MV compounds the electronic situation is quite clear (e.g., *N,N,N′,N′*-tetraalkylphenylenediamine radical cations[22,23] belong to class III), the situation remained cumbersome for others for many years (e.g., the Creutz-Taube salt)[13] or is still under debate (e.g., *N,N,N′,N′*-tetraanisylphenylenediamine radical cation).[15,24,25] While some of us derived for the latter cation a small though significant barrier from optical spectra using the semiclassical one-mode Marcus−Hush theory,[15] Coropceanu et al.[26] found this cation to be delocalized by vibronic coupling calculations using the full dynamic solutions in the diabatic approximation. The confusion arises because class III compounds are believed to have narrow charge resonance absorption lines with vibrational progression visible (e.g., in *N,N,N′,N′*-tetraalkylphenylenediamine radical cations)[22,23] while typical class II compounds show a broad featureless IV-CT band similar to the one observed in *N,N,N′,N′*-tetraanisylphenylenediamine radical cation.

However, mode-specific information is generally difficult to extract from the IV-CT or charge resonance absorption band shape due to severe solvent-induced broadening and/or fast photochemistry in the excited state. Resonance Raman spectroscopy[27] (RR) provides specific information on the molecular degrees of freedom involved in the initial structural changes of photochemically active systems. Moreover, it is a reliable tool for investigating the symmetry, equilibrium geometry, and dynamics of the resonantly excited electronic state. To gain more insight into the vibrations involved in the charge transfer of MV systems, and, thus, into the absorption band shape, extensive resonance Raman spectroscopical studies were carried out previously by several research groups.[28−30] A time-dependent formalism[31−33] has been applied to interpret the RR scattering activities and absorption cross section and to determine the Franck−Condon parameters of the vibrational modes coupled to the intensive charge-transfer band in asymmetrical[34,35] and symmetrical inorganic mixed-valence compounds.[36−41] Recently, the attention has been directed also toward organic[22,42] charge-transfer systems.

The special interest in triarylamine-based radical cations and their electronic nature stems from their wide application as hole transport molecules in optoelectronic materials[43,44] and their use as high-spin compounds in organic magnets.[45,46] But they have

(10) Badger, B.; Brocklehurst, B. *Trans. Faraday Soc.* **1970**, *66*, 2939−2947.
(11) Braun-Sand, S. B.; Wiest, O. *J. Phys. Chem. B* **2003**, *107*, 9624−9628.
(12) Ito, T.; Hamaguchi, T.; Nagino, H.; Yamaguchi, T.; Washington, J.; Kubiak, C. *Science* **1997**, *277*, 660−663.
(13) Demadis, K. D.; Hartshorn, C. M.; Meyer, T. J. *Chem. Rev.* **2001**, *101*, 2655−2685.
(14) Nelsen, S. F. *Chem. Eur. J.* **2000**, *6*, 581−588.
(15) Lambert, C.; Nöll, G. *J. Am. Chem. Soc.* **1999**, *121*, 8434−8442.
(16) Lindeman, S. V.; Rosokha, S. V.; Sun, D.; Kochi, J. K. *J. Am. Chem. Soc.* **2002**, *124*, 843−855.
(17) Roeder, J. C.; Meyer, F.; Hyla-Kryspin, I.; Winter, R. F.; Kaifer, E. *Chem. Eur. J.* **2003**, *9*, 2636−2648.
(18) Demadis, K. D.; Neyhart, G. A.; Kober, E. M.; White, P. S.; Meyer, T. J. *Inorg. Chem.* **1999**, *38*, 5948−5959.
(19) Rocha, R. C.; Toma, H. E. *Inorg. Chim. Acta* **2000**, *310*, 65−80.
(20) Stadler, C.; Daub, J.; Koehler, J.; Saalfrank, R. W.; Coropceanu, V.; Schuenemann, V.; Ober, C.; Trautwein, A. X.; Parker, S. F.; Poyraz, M.; Inomata, T.; Cannon, R. D. *J. Chem. Soc., Dalton Trans.* **2001**, 3373−3383.
(21) Londergan, C. H.; Rocha, R. C.; Brown, M. G.; Shreve, A. P.; Kubiak, C. P. *J. Am. Chem. Soc.* **2003**, *125*, 13912−13913.
(22) Bailey, S. E.; Zink, J. I.; Nelsen, S. F. *J. Am. Chem. Soc.* **2003**, *125*, 5939−5947.
(23) Nelsen, S. F.; Tran, H. Q.; Nagy, M. A. *J. Am. Chem. Soc.* **1998**, *120*, 298−304.
(24) Coropceanu, V.; Malagoli, M.; Andre, J. M.; Bredas, J. L. *J. Am. Chem. Soc.* **2002**, *124*, 10519−10530.
(25) Utz, N.; Koslowski, T. *Chem. Phys.* **2002**, *282*, 389−397.
(26) Coropceanu, V.; Lambert, C.; Nöll, G.; Brédas, J.-L. *Chem. Phys. Lett.* **2003**, *373*, 153.
(27) Myers, A. B. In *Laser Techniques in Chemistry*; Myers, A. B., Rizzo, T. R., Eds.; John Woley & Sons: New York, 1995; Vol. XXIII, pp 325−384.
(28) Hupp, J. T.; Williams, R. D. *Acc. Chem. Res.* **2001**, *34*, 808−817.
(29) Talaga, D. S.; Zink, J. I. *J. Phys. Chem. A* **2001**, *105*, 10511−10519.
(30) Watson, D. F.; Bocarsly, A. B. *Coor. Chem. Rev.* **2001**, *211*, 177−194.
(31) Heller, E. J. *Acc. Chem. Res.* **1981**, *14*, 368−375.
(32) Heller, E. J.; Sundberg, R.; Tannor, D. *J. Phys. Chem.* **1982**, *86*, 1822−1833.
(33) Lee, S.-Y.; Heller, E. J. *J. Chem. Phys.* **1979**, *71*, 4777−4788.
(34) Doorn, S. K.; Hupp, J. T. *J. Am. Chem. Soc.* **1989**, *111*, 4704−4712.
(35) Tominaga, K.; Kliner, D. A. V.; Johnson, A. E.; Levinger, N. E.; Barbara, P. F. *J. Chem. Phys.* **1993**, *98*, 1228−1243.
(36) Doorn, S. K.; Hupp, J. T.; Porterfield, D. R.; Campion, A.; Chase, D. B. *J. Am. Chem. Soc.* **1990**, *112*, 4999−5002.
(37) Petrov, V.; Hupp, J. T.; Mottley, C.; Mann, L. C. *J. Am. Chem. Soc.* **1994**, *116*, 2171−2172.
(38) Lu, H.; Petrov, V.; Hupp, J. T. *Chem. Phys. Lett.* **1995**, *235*, 521−527.
(39) Williams, R. D.; Petrov, V. I.; Lu, H. P.; Hupp, J. T. *J. Phys. Chem. A* **1997**, *101*, 8070−8076.
(40) Sando, G. M.; Spears, K. G.; Hupp, J. T.; Ruhoff, P. T. *J. Phys. Chem. A* **2001**, *105*, 5317−5325.
(41) Marin, T. W.; Homoelle, B. J.; Spears, K. G.; Hupp, J. T.; Spreer, L. O. *J. Phys. Chem. A* **2002**, *106*, 1131−1143.
(42) Williams, R. D.; Hupp, J. T.; Ramm, M. T.; Nelsen, S. F. *J. Phys. Chem. A* **1999**, *103*, 11172−11180.
(43) Strohriegl, P.; Grazulevicius, J. V. *Adv. Mater.* **2002**, *14*, 1439−1452.
(44) Koene, B. E.; Loy, D. E.; Thompson, M. E. *Chem. Mater.* **1998**, *10*, 2235−2250.
(45) Blackstock, S. C.; Selby, T. D. In *Magnetic Properties of Organic Materials*; Lahti, P. M., Ed.; Marcel Dekker: New York, 1999; pp 165−178.

also features which make them almost ideal systems for the study of intramolecular ET processes: they are easily accessible via Pd-catalyzed CC and CN bond couplings, the bridge connecting the two triarylamine moieties can be varied over a broad range, the local redox potentials of the triarylamine moieties can be tuned by substituents, and the bis(triarylamine) MV species possess a relatively low reorganization energy which makes the optically induced ET to be in the NIR, well-separated from other electronic excitations.[15,47−55]

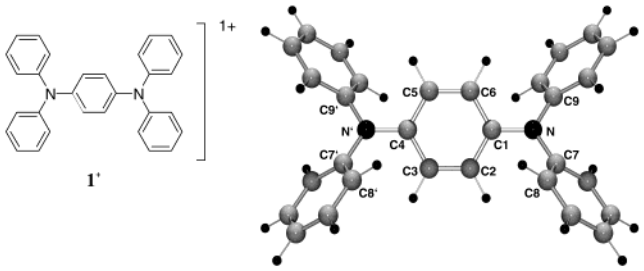

The smallest bis(triarylamine) MV species conceivable is *N*,*N*,*N*′,*N*′-tetraphenylphenylenediamine radical cation $\mathbf{1}^+$. It is the aim of this paper to collect and compare electronic, structural, and spectroscopic data on $\mathbf{1}^+$ in order to clarify the electronic situation. We will first discuss the crystal structure as derived from X-ray diffraction and will compare these data with DFT calculations. We will then present a simple two-state two-mode model within the semiclassical Marcus−Hush theory in order to interpret the optical spectra. Finally we will assign IR and Raman spectra of $\mathbf{1}^+$ by comparison with DFT-calculated vibrations and we will present resonance Raman spectra which give insight into the modes involved in the ET process. A detailed resonance Raman intensity analysis within the time-dependent formalism[31−33] will be presented in order to determine the reorganization energy upon optical excitation.

Results and Discussion

A. Structural Properties: X-ray Structure Analysis and DFT Calculations. The radical cation $\mathbf{1}^+$ was synthesized by oxidation of *N*,*N*,*N*′,*N*′-tetraphenylphenylenediamine with $SbCl_5$ in CH_2Cl_2. After removal of the solvent a green-blue solid was obtained. This solid was recrystallized from THF, yielding crystals with the composition $\mathbf{1}^+SbCl_6^-(THF)_{0.5}$ which were suitable for single-crystal X-ray diffraction analysis. The crystal structure shows two independent cations, both having a crystallographic inversion center which makes the point group C_i but with only little deviations from C_{2h}. However, the THF molecule which was incorporated in the crystal shows very strong thermal ellipsoids indicating disorder. Therefore, we recrystallized the salt from CH_2Cl_2/dioxane and obtained crystals with the composition $\mathbf{1}^+SbCl_6^-(dioxane)_{0.5}$. The crystal structure of this salt is very similar to the one of $\mathbf{1}^+SbCl_6^-(THF)_{0.5}$. In particular the two independent cations show a crystallographic inversion center and the symmetry is almost C_{2h}. As expected the dioxane molecule is not disordered and has small displacement parameters. Important distances and angles for $\mathbf{1}^+SbCl_6^-(dioxane)_{0.5}$ are collected in Table 1; the parameters for $\mathbf{1}^+SbCl_6^-(THF)_{0.5}$ are collected in the Supporting Information. The distances and angles of the in total four independent cations vary only little (see Supporting Information). Comparison of the C−C and C−N bond length of the radical cations with those of the neutral *N*,*N*,*N*′,*N*′-tetraphenylphenylenediamine **1** (crystallographic C_i symmetry with strong deviations from C_{2h} for two independent molecules in the unit cell; the parameters of only one molecule are given in Table 1, the parameters of the other molecule can be found in the Supporting Information) shows that the radical cation has a quinoidal distortion. The nitrogen centers are trigonal planar coordinate, the angle sum is 360°. The aryl rings are arranged in propeller form around the nitrogen centers as observed in other triarylamine radical cations.[56−58]

Table 1. Selected Distances (Å) and Angles of $\mathbf{1}^+$ and of **1** Determined by X-ray Crystallography as Well as DFT Calculated Values

	1	BPW91 **1**(C_{2h})	$\mathbf{1}^+SbCl_6^-(dioxane)_{0.5}$	BPW91 $\mathbf{1}^+$ (C_{2h})
C2−C3	1.387(4)	1.396	1.351(2)	1.385
C6−C1	1.389(4)	1.412	1.416(2)	1.424
C1−C2	1.387(4)	1.412	1.418(2)	1.424
C1−N	1.433(3)	1.425	1.363(2)	1.397
N−C7	1.405(4)	1.425	1.444(2)	1.432
N−C9	1.426(3)	1.425	1.430(2)	1.432
C9−N−C1	121.2(2)	119.93	120.90(15)	120.68
C9−N−C7	121.9(2)	120.12	116.53(14)	118.64
C7−N−C1	116.8(2)	119.93	122.54(15)	120.68
C7−N−N′−C9′	180	180	180	180
C7−N−N′−C7′	−3.3	0	−4.4	0
C2−C1−N−C7	−53.8	−40.99	−8.6	−29.97
C1−N−C7−C8	−55.7	−45.57	−64.0	−39.90

For comparison with the X-ray structure analysis we also performed DFT calculations on $\mathbf{1}^+$ and **1** with the Gaussian98[59] program package. The structures, vibrational characteristics, IR intensities, and Raman scattering activities of the radical cation were computed. The molecular structures were optimized at the UBPW91 level of theory requiring the Becke's 1988 exchange and Perdew and Wang's 1991 gradient-corrected correlation functionals. The 6-31G* split valence plus polarization basis set was used. Unlike UHF calculations, which are highly spin

(46) Bushby, R.-J. In *Magnetism: Molecules to Materials II*; Miller, J. S., Drillon, M., Eds.; Wiley-VCH: Weinheim, Germany, 2001; pp 149−187.
(47) Bonvoisin, J.; Launay, J.-P.; Van der Auweraer, M.; De Schryver, F. C. *J. Phys. Chem.* **1994**, *98*, 5052−5057 (see also correction **1996**, *100*, 18 006).
(48) Bonvoisin, J.; Launay, J.-P.; Verbouwe, W.; Van der Auweraer, M.; De Schryver, F. C. *J. Phys. Chem.* **1996**, *100*, 17 079−17 082.
(49) Lambert, C.; Gaschler, W.; Schmälzlin, E.; Meerholz, K.; Bräuchle, C. *J. Chem. Soc., Perkin Trans. 2* **1999**, 577−588.
(50) Lambert, C.; Nöll, G. *Synth. Met.* **2003**, *139*, 57−62.
(51) Lambert, C.; Nöll, G. *Angew. Chem., Int. Ed.* **1998**, *37*, 2107−2110.
(52) Lambert, C.; Nöll, G. *Chem. Eur. J.* **2002**, *8*, 3467−3477.
(53) Lambert, C.; Nöll, G. *J. Chem. Soc., Perkin Trans. 2* **2002**, 2039−2043.
(54) Lambert, C.; Nöll, G.; Hampel, F. *J. Phys. Chem. A* **2001**, *105*, 7751−7758.
(55) Lambert, C.; Nöll, G.; Schelter, J. *Nat. Mater.* **2002**, *1*, 69−73.
(56) Brown, G. M.; Freeman, G. R.; Walter, R. I. *J. Am. Chem. Soc.* **1977**, *99*, 6910−6915.
(57) Sobolev, A. N.; Bel'skii, V. K.; Romm, I. P.; Chernikova, N. Y.; Guryanova, E. N. *Acta Crystallogr., Sect. C: Cryst. Struct. Commun.* **1985**, *C41*, 967−971.
(58) Low, P. J.; Paterson, M. A. J.; Puschmann, H.; Goeta, A. E.; Howard, J. A. K.; Lambert, C.; Cherryman, J.; Tackley, D. R.; Leeming, S.; Brown, B. *Chem. Eur. J.* **2004**, *10*, 83.
(59) Frisch, M. J.; Trucks, G. W.; Schlegel, H. B.; Scuseria, G. E.; Robb, M. A.; Cheeseman, J. R.; Zakrzewski, V. G.; Montgomery, J. A.; Stratmann, R. E.; Burant, J. C.; Dapprich, S.; Millam, J. M.; Daniels, A. D.; Kudin, K. N.; Strain, M. C.; Farkas, O.; Tomasi, J.; Barone, V.; Cossi, M.; Cammi, R.; Mennucci, B.; Pomelli, C.; Adamo, C.; Clifford, S.; Ochterski, J.; Peterson, G. A.; Ayala, P. Y.; Cui, Q.; Morokuna, K.; Malick, D. K.; Rabuck, A. D.; Raghavachari, K.; Foresman, J. B.; Cioslowski, J.; Ortiz, J. V.; Baboul, A. G.; Stefanov, B. B.; Liu, G.; Liashenko, A.; Piskorz, P.; Komaromi, I.; Gomperts, R.; Martin, R. L.; Fox, D. J.; Keith, T.; Al-Laham, M. A.; Peng, C. Y.; Nanayakkara, A.; Gonzalez, C.; Challacombe, M.; Gill, P. M. W.; Johnson, B.; Chen, W.; Wong, M. W.; Andres, J. L.; Gonzales, C.; Head-Gordon, M. *Gaussian 98*, revision A.7; Gaussian Inc.: Pittsburgh, PA, 1998.

contaminated, the DFT calculations are almost free of any spin contamination ($S^2 = 0.753$). The fully optimized molecular geometries correspond to minima on the ground-state potential surface of $\mathbf{1}^+$ and **1**, as was proven by normal-mode analysis, employing the analytically calculated Hessian. The molecular structures of $\mathbf{1}^+$ and **1** computed with symmetry restrictions resulted in structural parameters almost identical to those calculated without symmetry restrictions. The bond length differences between the two procedures are smaller than 0.001 Å. For $\mathbf{1}^+$ we found two minima close in energy with D_2 and C_{2h} symmetry, the latter involving a center of inversion. The X-ray structure analysis of $\mathbf{1}^+$ showed that the molecular structure in the solid state has C_{2h} symmetry. Moreover, the C_{2h} symmetric cation is predicted by the quantum chemical calculations to be more stable (by 2.6 kJ/mol) than the D_2 symmetric form. These two conformers differ in the relative helicity of the two triarylamine propellers. Selected DFT-computed parameters of the cation are included in Table 1 and are in good agreement with the experimentally observed values. The computed molecular parameters for the neutral species and the radical cation mainly differ in the bonds and angles involving the central benzene and the nitrogen atoms. The C−N bond is significantly reduced in the cation, compared to the neutral form. As mentioned before, removing an electron from **1** stabilizes the C_{2h} symmetric cation $\mathbf{1}^+$ with respect to the D_2 symmetric form. However, in the case of the neutral compound **1** the D_2 symmetric form has been found to be slightly more stable (by 0.03 kJ/mol) than the C_{2h} symmetric isomer but which is of course insignificant.

Both the X-ray structure analysis and the DFT calculations indicate a centrosymmetric structure of $\mathbf{1}^+$. However, the unambiguous conclusion of a delocalized class III structure for $\mathbf{1}^+$ cannot be drawn from these investigations for several reasons: (1) the investigations refer to either the solid state or the gas phase and not to solution where time and density fluctuations of the solvent may induce a certain degree of asymmetry in $\mathbf{1}^+$. (2) Cation $\mathbf{1}^+$ might be slightly asymmetric in the solid state and the crystallographic symmetry is due to static or dynamic disorder. (3) The symmetry of $\mathbf{1}^+$ in the solid state might be induced by the position of the $SbCl_6^-$ gegenion which sits right above the middle of the cation.[60] (4) DFT methods are known to overemphasize delocalization in radical ions.[61,62]

B. Optical Properties: UV/Vis/NIR Spectroscopy and Theoretical Description of the Potential Energy Surface. The UV/vis/NIR absorption spectra of $\mathbf{1}^+$ were recorded in CH_2Cl_2 and in MeCN solution (see Figure 2). The spectrum in MeCN is almost identical to the one (not shown) in EtCN with 0.2 tetrabutylammoniumhexafluorophosphate (TBAH) as supporting electrolyte from ref 26.

The broad and strong absorption in the NIR around 12000 cm^{-1} might be termed either a "charge resonance band" (in the case of class III) or a "intervalence charge-transfer band" (in the case of class II). As we will show later, $\mathbf{1}^+$ belongs to class III right at the border to class II, and therefore, "charge resonance" will be used to name the NIR absorption. To fit the experimental charge resonance bands in the two solvents and to obtain the parameters which govern the ground- and excited-state potential energy surfaces (PES), we applied the semiclassical Marcus−Hush theory[8] for the degenerate case. It is important to note that the model used is equally applicable to both localized (Robin−Day class II) and delocalized (Robin−Day class III) systems in order not to prejudice the outcome of the band fit by the choice of the model.[9,14,63−65] In our modification,[58] we used a vibronic matrix (eq 1) with one asymmetric mode x (the ET coordinate in the conventional Marcus−Hush theory) and, in addition, one totally symmetric mode y similar to the one given by Piepho,[67] Schatz,[68] Hush,[69,70] and Zink.[29] This vibronic matrix with the matrix elements $H_{ij} = \langle\varphi_i|\hat{\mathbf{H}}|\varphi_j\rangle$ is presented here in the localized electronic basis where the basis functions φ represent diabatic (noninteracting) states in which the excess hole is localized at one of the two redox centers as given in eq 22 by Reimer and Hush.[69] The diabatic potentials are expanded as power series which are terminated after the quadratic terms for the diagonal elements and after the linear terms for the off-diagonal elements. In this matrix, V is the electronic coupling, λ_x and λ_y are the reorganization energies for the x and y mode, respectively, and l_x and l_y are the linear vibronic coupling constants. The term $V + l_y y$ in the diagonal elements places the transition state at the coordinate $x = 0$, $y = 0$ at energy = 0. The fact that a term $l_y y$ appears in the off-diagonal element of eq 1 produces a mode-dependent coupling as outlined in refs 29 and 67−69. The (dimensionless) displacement of the upper adiabatic surface and the ground-state surface along the y mode is given by $\Delta_y =$

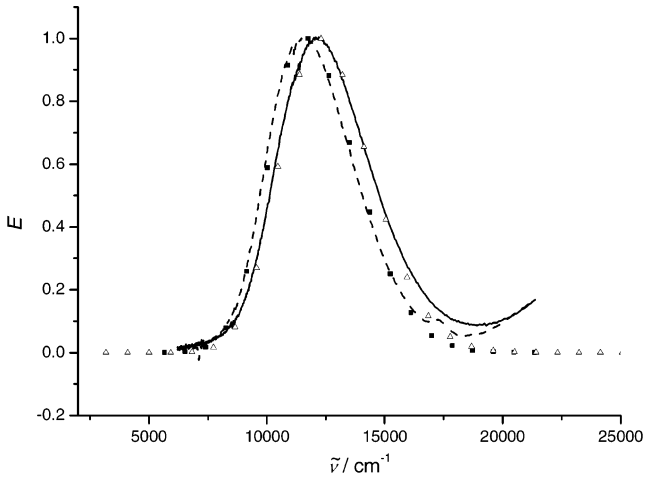

Figure 2. Normalized UV/vis/NIR absorption spectra of $\mathbf{1}^+SbCl_6^-(THF)_{0.5}$ in MeCN (solid line) and CH_2Cl_2 (dashed line) as well as the fitted spectra (open triangles and solid rectangles) by the two-mode approach.

(60) Kochi et al. quite recently reported a MV compound that shows a symmetrical charge distribution in the solid state but is asymmetrically localized in solution: Sun, D.-L.; Rosokha, S. V.; Lindeman, S. V.; Kochi, J. K. *J. Am. Chem. Soc.* **2003**, *125*, 15950−15963.
(61) Jones, G. A.; Carpenter, B. K.; Paddon-Row, M. N. *J. Am. Chem. Soc.* **1999**, *121*, 11171−11178.
(62) Blomgren, F.; Larsson, S.; Nelsen, S. F. *J. Comput. Chem.* **2001**, *22*, 655−664.
(63) Cave, R. J.; Newton, M. D. *Chem. Phys. Lett.* **1996**, *249*, 15−19.
(64) Creutz, C.; Newton, M. D.; Sutin, N. *J. Photochem. Photobiol. A: Chem.* **1994**, *82*, 47−59.
(65) Newton, M. D. *Adv. Chem. Phys.* **1999**, *106*, 303−375.
(66) Deleted in proof.
(67) Piepho, S. B. *J. Am. Chem. Soc.* **1988**, *110*, 6319−6326.
(68) Schatz, P. N. In *Mixed Valency Systems: Applications in Chemistry, Physics and Biology*; Prassides, K., Ed.; Kluwer Academic Publishers: Dordrecht, Holland, 1991; pp 7−28.
(69) Reimers, J. R.; Hush, N. S. *Chem. Phys.* **1996**, *208*, 177−193.
(70) Hush, N. S. In *Mixed Valence Compounds 151*; Brown, D. B., Ed.; D. Reidel Publishing Co.: Dordrecht, Holland, 1980; p 151.

l_y/λ_y and along the x mode it is $\Delta_x = l_x/2\lambda_x$. Thus, choosing $l_x = \lambda_x$ places the minima of the diabatic potentials at $x = \pm 0.5$. Furthermore, we make the simplification that $\lambda_x = \lambda_y = \lambda$. The variable displacement of the minima along the y mode results in an effective reorganization energy $L = l_y^2/\lambda$ (see Figure 1, diagram on the right-hand side). Diagonalization of the matrix gives two adiabatic potential energy surfaces. We calculated the absorption spectra using a Boltzmann distribution of infinitesimally spaced vibrational states for both the ground and excited state and the energy difference between the two adiabatic potential energy surfaces.[8] As long as the coupling V is rather strong, the spectra can only be accurately fitted by adjusting V, l_y, and λ and, thus, no assumptions about any effective (diabatic) electron-transfer distance are necessary as in the traditional one-dimensional Marcus−Hush theory.

$$\begin{vmatrix} V + l_x x + \lambda_x x^2 + l_y y + \lambda_y y^2 - \epsilon & V + l_y y \\ V + l_y y & V - l_x x + \lambda_x x^2 + l_y y + \lambda_y y^2 - \epsilon \end{vmatrix} = 0 \quad (1)$$

$$\tilde{\nu}_{1/2}(\mathrm{HTL}) = [16 \ln(2) k_b T \tilde{\nu}_{\max}]^{1/2} \quad (2)$$

$$V = \frac{\mu_{\mathrm{eg}} \cdot \tilde{\nu}_{\max}}{\Delta\mu_{\mathrm{ab}}} \quad (3)$$

$$\mu_{\mathrm{eg}} = 0.09584 \sqrt{\frac{\int \epsilon(\tilde{\nu})\, \mathrm{d}\tilde{\nu}}{\tilde{\nu}_{\max}}} \quad (4)$$

$$\Delta\mu_{\mathrm{ab}} = \sqrt{\Delta\mu_{\mathrm{eg}}{}^2 + 4\mu_{\mathrm{eg}}{}^2} \quad (5)$$

If V is rather small, the spectra in our two-mode approach become Gaussian-shaped (with the bandwidth at half height at the high-temperature limit (HTL) given by eq 2) and independent of V and l_y, and the solutions are equivalent to the traditional one-dimensional Marcus−Hush theory. In this case, an estimate of the adiabatic (or diabatic) dipole moment difference between the adiabatic (or diabatic) states is still necessary in order to calculate V by eq 3 (generalized Mulliken-Hush theory[63−65]). In this equation $\tilde{\nu}_{\max}$ is the energy of the electronic transition, μ_{eg} is the transition moment of the IV-CT band which can be calculated by eq 4, and $\Delta\mu_{\mathrm{ab}}$ is the diabatic dipole moment difference which can be traced back to purely adiabatic quantities by eq 5 where $\Delta\mu_{\mathrm{eg}} = \mu_{\mathrm{e}} - \mu_{\mathrm{g}}$ is the adiabatic dipole moment difference. In principle, this adiabatic dipole moment difference can be measured by Stark spectroscopy[71−75] or can be computed by quantum chemical methods.[76,77] The usual method however is to estimate either the diabatic or the adiabatic dipole moment difference by $e \times r$ where r is the distance between the redox centers. While for strongly localized systems this estimation is rather accurate it becomes worse the stronger the delocalization is. Especially for triarylamine based systems,

Table 2. Parameters [cm^{-1}] Used To Fit the Experimental Charge Resonance Band

	$\tilde{\nu}_{\max}$	V	λ	l_y	$L = l_y^2/\lambda$	ΔG^*
CH_2Cl_2	11 580	5300	12 000	7000	4080	60
MeCN	12 140	5500	12 600	7200	4110	80
EtCN/0.2 M TBAH	12 060	5600	12 200	7200	4250	30
EtCN/0.2 M TBAH[a]	12 060	5600	12 200	5400	2390	30
EtCN/0.2 M TBAH[b]	12 060	3630	12 060	0	0	480

[a] Calculated by the full dynamic solution in the diabatic approximation, see ref 26. [b] Calculated by the one-dimensional Marcus−Hush theory, see ref 26.

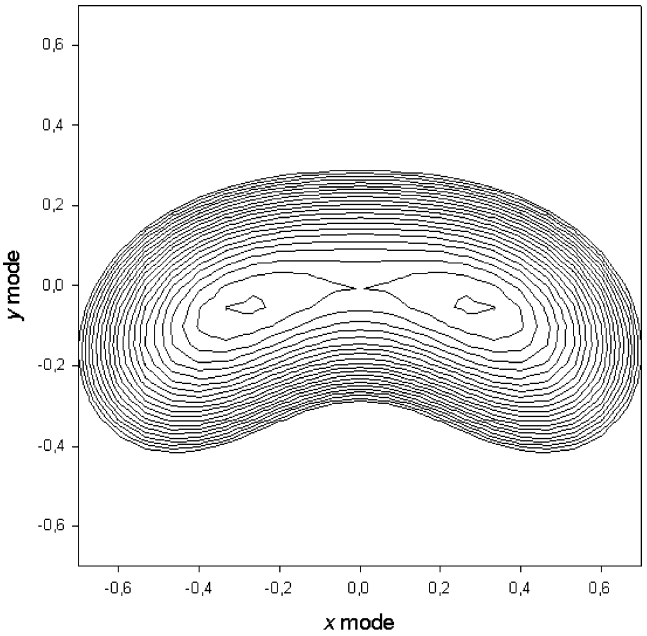

Figure 3. Contour plot of the ground-state PES of $\mathbf{1}^+$ as derived from the two-mode Marcus−Hush analysis. The contour lines are spaced by 50 cm^{-1}.

Nelsen et al. quite recently showed that using the nitrogen−nitrogen distance leads to a gross overestimation of the adiabatic ET distance.[78] Thus, especially for species at the class II/III transition the two-mode model is a distinct improvement.

The results for the fits in Figure 2 are given in Table 2 together with the results from the work of Coropceanu et al.[26] using the full dynamic solutions and the results from the one-dimensional Marcus−Hush analysis using eq 3 for the evaluation of V and the N−N distance (5.6 Å) and $\mu_{\mathrm{eg}} = 8.1$ D. Neither the electronic coupling V nor the reorganization energy strongly depend on the solvent which is a strong hint toward a delocalized system.[79] For both the traditional one-mode and the two-mode Marcus−Hush theory, the ET barrier ΔG^* vanishes if $2V > \lambda$. While this is obviously the case for $\mathbf{1}^+$ if we apply the two-mode model ($\Delta G^* < 80$ cm^{-1}), i.e., we are right at the transition between class II and III, it is not if we use the one-mode model which yields a significant barrier (480 cm^{-1}) because of the much smaller V derived from eq 3.

In Figure 3 the contour plot of the adiabatic ground-state PES for $\mathbf{1}^+$ in CH_2Cl_2 as obtained by the two-mode analysis is given. It can easily be seen that there is practically no barrier for the

(71) Hupp, J. T.; Dong, Y.; Blackbourn, R. L.; Lu, H. *J. Phys. Chem.* **1993**, *97*, 3278−3282.
(72) Bublitz, G. U.; Laidlaw, W. M.; Denning, R. G.; Boxer, S. G. *J. Am. Chem. Soc.* **1998**, *120*, 6068−6075.
(73) Ferretti, A.; Lami, A.; Murga, L. F.; Shehadi, I.; Ondrechen, M. J.; Villani, G. *J. Am. Chem. Soc.* **1999**, *121*, 2594−2596.
(74) Oh, D. H.; Sano, M.; Boxer, S. G. *J. Am. Chem. Soc.* **1991**, *113*, 6880−6890.
(75) Shin, Y.-g. K.; Brunschwig, B. S.; Creutz, C.; Sutin, N. *J. Am. Chem. Soc.* **1995**, *117*, 8668−8669.
(76) Nelsen, S. F.; Blomgren, F. *J. Org. Chem.* **2001**, *66*, 6551−6559.
(77) Nelsen, S. F.; Newton, M. D. *J. Phys. Chem. A* **2000**, *104*, 10023−10031.
(78) Nelsen, S. F.; Konradsson, A. E.; Luo, Y.; Kim, K.-Y.; Blackstock, S. C. Submitted for publication.
(79) Possible effects of ion pairing which is likely to occur in methylene chloride but unlikely in MeCN are ignored in our case. See: Nelsen S. F.; Ismagilov, R. F. *J. Phys. Chem. A* **1999**, *103*, 5373.

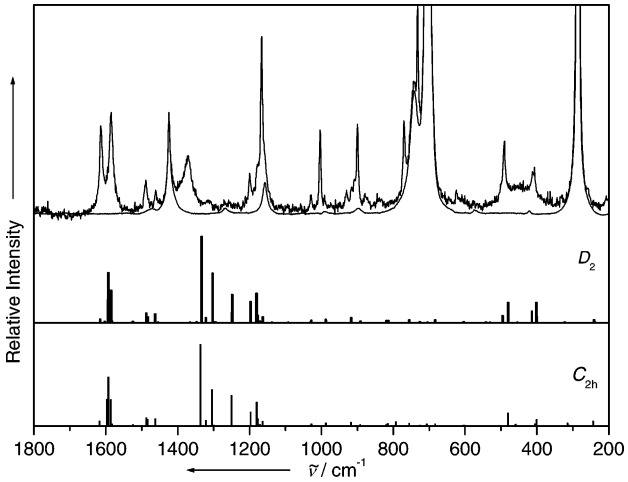

Figure 4. Calculated Raman scattering intensities at the BPW91/6-31G-(d) level for $\mathbf{1}^+$ and the off-resonance Raman spectrum in CH_2Cl_2 solution measured at 514.5 nm excitation. The spectrum of the pure CH_2Cl_2 solvent is also given as a thin solid line.

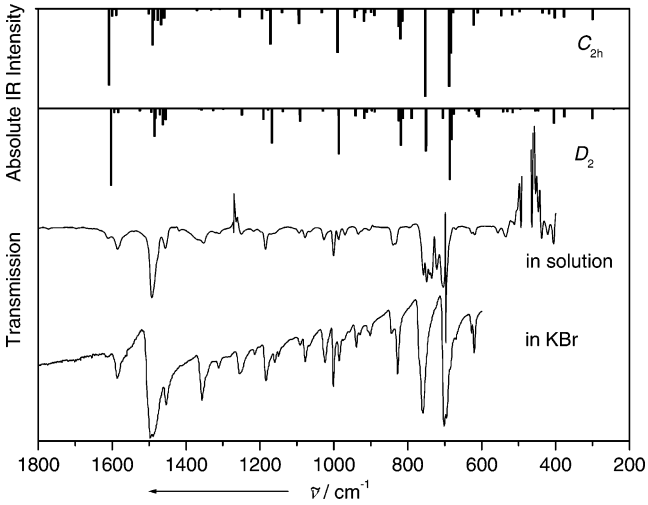

Figure 5. Calculated IR intensities at the BPW91/6-31G(d) level for $\mathbf{1}^+$ and the IR spectrum recorded in CH_2Cl_2 solution and in KBr matrix.

ET pathway which proceeds in a bent fashion rather than straight along the *x* axis. That broad absorption features are observed rather than the expected narrow lines with vibrational progression is due to the strong coupling to an average symmetric mode.[24]

C. IR and Raman Spectra and Their DFT Computation. To investigate the vibrational modes involved in the charge resonance excitations of $\mathbf{1}^+$ we performed a detailed vibrational study. This involved the measurement of the IR, off resonance and resonance Raman spectra, the assignment of IR and Raman vibrational modes by comparison with DFT computed vibrations, and the resonance Raman intensity analysis in order to determine the Franck−Condon parameters.

The vibrational spectroscopic techniques IR and Raman spectroscopy represent one of the most useful tools for obtaining information about the structure and properties of molecules from their vibrational transitions. However, the assignment of the infrared and Raman bands of polyatomic molecules is rather complicated. Theoretical calculations, first of all DFT calculations, are therefore the appropriate tools to obtain a deeper insight into the microscopic atomic displacements of complicated molecules.

To obtain structural information for $\mathbf{1}^+$, IR and Raman spectra of $\mathbf{1}^+$ in CH_2Cl_2 solution were measured. The IR spectrum of $\mathbf{1}^+$ was recorded also in a KBr matrix.

The Raman scattering activities of $\mathbf{1}^+$ were calculated maintaining the symmetry restrictions (C_{2h} or D_2) because of the high computational costs. The Raman scattering activities were converted into Raman scattering intensities for the 514.5 nm off-resonant excitation line as described by Porezag and Pederson.[80]

The off-resonance Raman spectrum of $\mathbf{1}^+$ in CH_2Cl_2 solution is shown in Figure 4 in comparison with the DFT-calculated Raman scattering intensities. The IR spectra of $\mathbf{1}^+$ measured in a KBr matrix and in solution are presented in Figure 5. The calculated vibrational frequencies (no scaling factors were applied) and IR intensities are in good agreement with the experimental data. For the Raman data, a general correspondence between the calculated and experimental intensities could be observed. However, the calculation of the polarizability derivatives, which is required to evaluate the Raman intensities, is very sensitive to the level of theory.[80] To get a better agreement between the experimentally observed Raman intensities and the calculated ones a higher level of theory is required, but then the numerical calculation of the Raman scattering activities would be extremely time-consuming. Therefore, we refrained from applying a higher level of theory.

The DFT calculations with D_2 and C_{2h} symmetry constraints yielded very similar results for the vibrational frequencies, infrared absorption intensities, and Raman scattering intensities (Figures 4 and 5). In the case of C_{2h} symmetry the IR active vibrational modes are forbidden in the Raman spectrum due to the center of inversion. However, the calculations with D_2 symmetry restrictions predicted a similar behavior. The IR active bands have almost zero Raman scattering activity, and vice versa. Thus, a definite conclusion about the symmetry of $\mathbf{1}^+$ (D_2 or C_{2h}) in solution cannot be drawn from our Raman and IR measurements; however, the excellent agreement of the IR spectra in solution and in the solid state (KBr matrix) where the structure is known by the X-ray crystal structure analysis on one hand and the good agreement of the calculated and computed spectra on the other hand suggests a symmetric and, therefore, a class III structure of $\mathbf{1}^+$ in which both nitrogen atoms are equivalent.

The vibrational analysis was carried out by comparing the computed vibrational modes with those obtained from the literature for benzene derivatives.[81] The vibrational assignment is given in Table 3. The corresponding computed wavenumbers are also listed. Upon substitution of the benzene molecule the symmetry is lowered and the degenerate vibrations are split into their counterparts.[81] A molecular structure of C_{2h} symmetry has a_g and b_g Raman and a_u and b_u IR active modes, while a molecular structure of D_2 symmetry has vibrational modes of a, b_1, b_2, and b_3 symmetry, which are Raman active. Only the a modes are IR inactive. The vibrational modes will be discussed in the following, taking into consideration a molecular structure of C_{2h} symmetry (see Table 3), but a strong correspondence

(80) Porezag, D.; Pederson, M. R. *Phys. Rev. B: Condens. Matter* **1996**, *54*, 7830−7836.

(81) Dollish, F. R.; Fateley, W. G.; Bentley, F. F. *Characteristic Raman Frequencies of Organic Compounds*; 1973.

Table 3. Experimental and Computed Vibrational Wavenumbers $\tilde{\nu}$, Displacement Parameters Δ, Vibrational Reorganization Energies $\lambda_{v,i}$, and Tentative Vibrational Assignment with DFT Results for the Most Prominent Vibrations of $\mathbf{1}^+$. Selected Values for $\mathbf{2}^+$ Are Given in Parentheses[22]

	$\tilde{\nu}$/cm^{-1}	$\tilde{\nu}$ DFT/cm^{-1}	Δ	$\lambda_{v,i}$/cm^{-1}	vibrational assignment[c]
IR	1585	1603 a_u			C═C stretch/phenyl e_{2g},[a] phenylene e_{1u}[a]
		1595 b_u			C═C stretch/phenyl e_{2g}[a]
		1588 a_u			C═C stretch/phenyl e_{2g}[b]
		1583 b_u			C═C stretch/phenyl e_{2g},[b] phenylene e_{1u}[b]
		1494 a_u			C═C stretch/phenyl, phenylene e_{1u}[a]
	1491	1486 b_u			C═C stretch/phenyl e_{1u},[a] phenylene e_{1u}[b] + C−N−C stretch
	1489	1482 a_u			C═C stretch/phenyl, phenylene e_{1u}[a] + sym C−N stretch
		1472 b_u			C═C stretch/phenylene e_{1u}[a] + asym C−N−C stretch
		1462 a_u			C═C stretch/phenyl e_{1u},[b] phenylene e_{1u}[a] + asym C−N stretch
	1454	1454 b_u			C═C stretch/phenyl, phenylene e_{1u}[b]
	1356	1366 a_u			sym C−N−C stretch + C═C stretch/phenyl e_{1u}[b]
		1366 b_u			asym C−N−C + C═C stretch/phenyl, phenylene e_{1u}[b]
		1346 b_u			sym C−N−C stretch + C═C stretch/phenylene e_{1u}[b]
	sh	1328 a_u			CCH deformation + sym C−N−C stretch
	1254	1250 b_u			C−N−C stretch + CCH deformation/phenylene e_{1u}[b]
	1184	1190 a_u			CCH deformation/phenyl e_{2g},[a] phenylene e_{1u}[a]
		1178 b_u			CCH deformation/phenyl e_{2g},[a] phenylene e_{1u}[b]
	1161	1171 a_u			CCH deformation/phenyl
	1150	1168 a_u			CCH deformation/phenyl e_{2g},[a] phenylene e_{1u}[a]
	1078	1092 a_u			CCH deformation/phenyl e_{1u}[b]
		1091 b_u			CCH deformation/phenyl e_{1u}[b]
	1024	1030 b_u			CCH deformation/phenyl e_{1u}[a]
	1001	987 a_u			phenyl trig. ring breathing + CCH deformation/phenylene
	826	817 a_u			out-of-plane CCH deformation
	758	751 b_u			out-of-plane CCH deformation
	702	686 a_u			out-of-plane CCH deformation
Raman	**1613** (1620)	1617 a_g	0.42 (0.64)	142.3 (335)	C═C stretch/phenyl, phenylene e_{2g}[a]
		1595 b_g			C═C stretch/phenyl e_{2g}[a]
	1582	1593 a_g	0.56	248.1	C═C stretch/phenyl e_{2g},[b] phenylene e_{2g}[a] + C−N stretch
		1586 a_g			C═C stretch/phenyl e_{2g},[b] phenylene e_{2g}[a] + C−N stretch
		1583 b_g			C═C stretch/phenyl, phenylene, e_{2g}[b]
	1489	1488 a_g	0.25	46.5	C═C stretch/phenyl e_{1u},[a] phenylene e_{2g}[a] + C−N−C stretch
		1484 b_g			C═C stretch/phenyl e_{1u}[a] + C−N−C stretch
	1461	1463 a_g	0.22	35.4	C═C stretch/phenyl e_{1u}[b] + C−N stretch + sym C−N−C stretch
		1455 b_g			C═C stretch/phenyl e_{1u},[b] phenylene e_{2g}[b]
	1365 (1368)	1337 a_g	1.20 (0.44)	982.8 (132)	sym N−Ar−N stretch
		1321 b_g			CCH deformation a_{2g} (Wilson 3, very weak usually)
		1305 a_g			sym N−Ar−N stretch
	1310 RR (1095)	1295 a_u			asym N−Ar−N stretch
		1197 a_g			CCH deformation/phenyl, phenylene e_{2g}[a] + C−N stretch
	1198	1180 a_g	0.64	245.4	CCH deformation/phenyl, phenylene e_{2g}[a] + C−N stretch
	1179	1177 a_g	0.43	109.0	CCH deformation/phenyl e_{2g}[a]
		1171 a_g			CCH deformation/phenyl e_{2g}[b]
	1166	1164 a_g			CCH deformation + phenylene ring stretch
	1030	1030 b_g			CCH deformation/phenyl e_{1u}[a]
		1028 a_g			CCH deformation/phenyl e_{1u}[a]
	1004	988 a_g			phenyl trig. ring breathing/b_{1u}
		987 b_g			phenyl trig. ring breathing b_{1u}
	sh	971 a_g			out-of-plane CCH deformation
	928	917 a_g			phenylene ring breathing/a_{1g} + C−N stretch
	898 (1014)	892 a_g	(0.47)	(112)	phenylene ring breathing/a_{1g}
	839	820 a_g			out-of-plane CCH deformation
		815 b_g			out-of-plane CCH deformation
	800 RR	793 a_g			out-of-plane phenylene deformation
	770	756 a_g			ring deformation/phenylene e_{2g}[a]
	732	725 a_g			ring deformation/phenyl, phenylene e_{2g}[a]
	491 (505)	480 a_g	1.34 (0.72)	440.8 (132)	C−N−C twist + in-plane phenylene deformation
	421	405 a_g			out-of-plane phenyl ring deformation
	409 (405)	401 b_g	1.24 (1.07)	314.4 (232)	out-of-plane phenyl ring deformation
	257	243 a_g	1.49	285.3	C−N−C (phenyl) twist + phenyl wagging
	205	194 a_g			phenylene out-of-plane deformation + N−Ar−N deformation

[a,b] Refer to the Wilson notation of the degenerate vibrations of the benzene molecule. The RR enhanced modes are marked as bold. [c] The benzene fundamentals from which the vibrational modes of $\mathbf{1}^+$ are derived.

between the molecular vibrations of the two symmetries has been observed (Figures 4 and 5).

Cation $\mathbf{1}^+$ consists of four identical monosubstituted (phenyl) benzene units and one disubstituted (phenylene) benzene unit. The computations showed that many vibrational modes involve only one type of the benzene rings, while others involve also the nitrogen atoms. Several vibrations are strongly coupled and involve the entire system. Scheme 1 presents selected vibrational modes and the corresponding Cartesian atomic displacements.

The splitting of the aromatic C═C stretch mode, which arises in the Raman spectrum of benzene[81] as a very strong band at 1596 cm^{-1} (Wilson numbers 8a and 8b, of e_{2g} symmetry) and

Scheme 1. The Cartesian Displacements of the Atoms during the Fundamental Resonance Enhanced Vibrations of $\mathbf{1}^+$

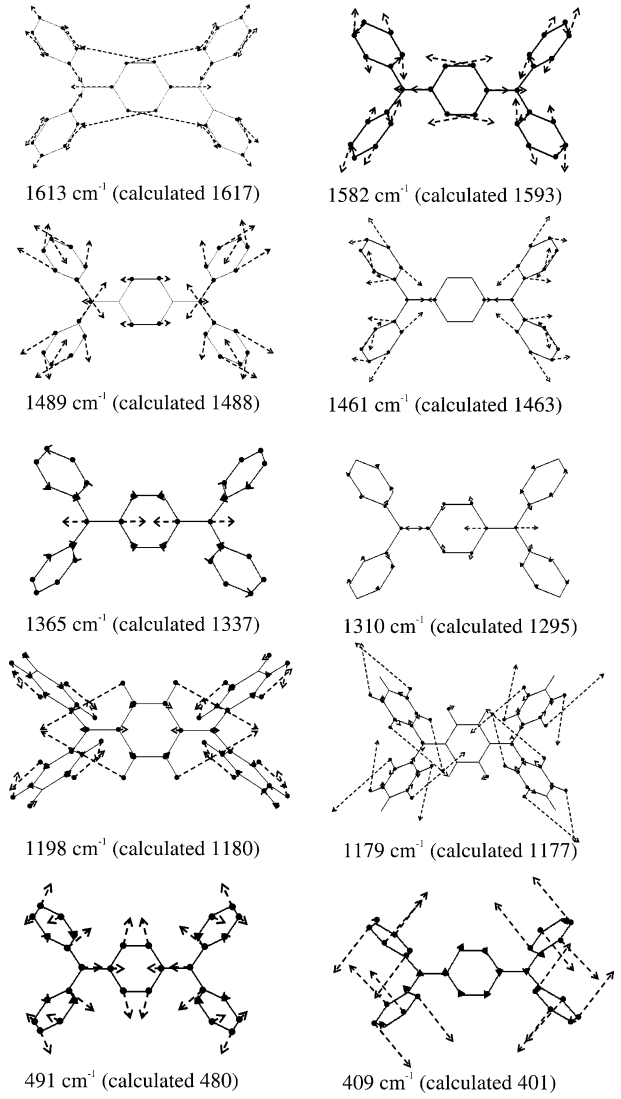

in the IR spectrum at 1486 cm^{-1} (Wilson numbers 19a and 19b, of e_{1u} symmetry), due to the lowering of symmetry leads to several Raman or IR active vibrations in this spectral region. In the off-resonance Raman spectrum of $\mathbf{1}^+$ (Figure 4) two vibrational modes at 1613 and 1582 cm^{-1} can be observed. The calculations (see Table 3) predicted several intense modes (1617, 1595, 1593, 1586 cm^{-1}) in this spectral region. The strongest vibration calculated at 1593 cm^{-1} (Scheme 1) corresponds to the symmetric aromatic stretch of the phenyl and phenylene rings and also involves the C−N bond. Raman bands due to C═C stretch vibrations also arise at 1489 and 1461 cm^{-1}, but with very weak intensity (Figure 4). The strong and broad band around 1490 cm^{-1} in the IR spectrum (Figure 5) probably consists of several C═C vibrational modes. The C═C stretch shows weak IR intensity around 1600 cm^{-1}.

The broad band at 1365 cm^{-1} in the off-resonance Raman spectrum of $\mathbf{1}^+$ can be assigned to a symmetric C−N stretching mode along the N−bridge−N axis. The largest atomic motions involved in this vibration are presented in Scheme 1.

The CCH deformation modes give rise to a strong Raman band (Figure 4) at 1166 and a shoulder at 1177 cm^{-1}. The vibration at 1198 cm^{-1} can be assigned to a CCH deformation

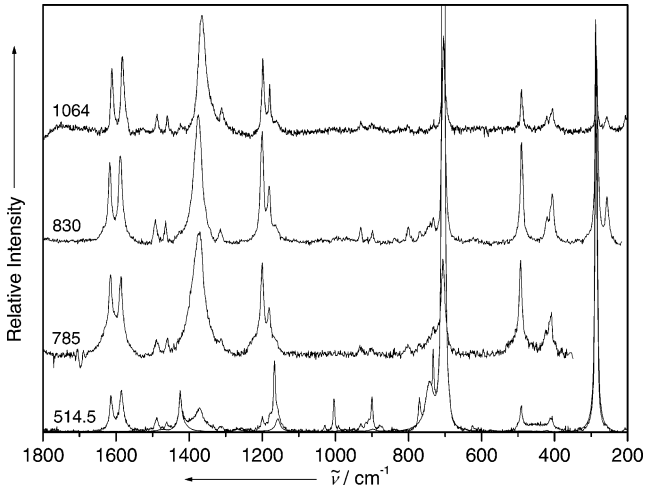

Figure 6. Resonance Raman spectra of $\mathbf{1}^+$ in CH_2Cl_2 solution measured at 1064, 830, and 785 nm excitation lines (top to bottom) in comparison with the off-resonance Raman spectrum at 514.5 nm.

band strongly coupled to the C−N stretching mode. The weak bands in the IR spectrum around 1150 cm^{-1} and the medium strong band at 1024 cm^{-1} are due to the CCH deformation modes.

The medium strong band at 1004 cm^{-1} in the Raman spectrum corresponds to the trigonal phenyl ring breathing mode, which derives its intensity from the benzene ring stretch of b_{1u} symmetry. Nevertheless, this mode is Raman allowed in $\mathbf{1}^+$ since the overall symmetry of the mode is a_g or b_g (see Table 3) as predicted by the calculations. A shoulder at higher wavenumbers can usually be observed in monosubstituted benzene derivatives and is attributed to CCH deformation. The benzene ring breathing of a_{1g} symmetry of the phenylene unit arises as a band of comparable intensity to the trigonale ring breathing mode at 898 cm^{-1}. The shoulder at 928 cm^{-1} has been attributed, based on our DFT calculations, also to a phenylene ring breathing mode, but coupled to a C−N stretch vibration.

The vibrational bands at 732 cm^{-1} in the Raman spectrum and at 758 cm^{-1} in the IR spectrum have been attributed to out-of-plane CCH deformation modes. The broad band in the IR spectrum of the solid form of $\mathbf{1}^+$ at 702 cm^{-1} has been accurately predicted by the computations and is also corresponding to an out-of-plane CCH deformation mode.

The Raman spectrum could be also recorded in the low wavenumber region. The CCN deformation mode arises at 491 cm^{-1}. The band at 409 cm^{-1} is mainly due to the out-of-plane deformation of the phenyl rings.

D. Resonance Raman Spectroscopy. Figure 6 presents the resonance Raman spectra of $\mathbf{1}^+$ in CH_2Cl_2 solution measured at 1064, 830, and 785 nm in comparison with the off-resonance spectrum recorded at 514.5 nm. We also performed Raman measurements for the neutral form **1**. These control experiments together with the nonresonant Raman measurements of $\mathbf{1}^+$ confirmed that scattering from the radical is strongly resonance enhanced if excitation wavelengths within the charge resonance band (see Figure 7) are applied. Moreover, changes in the relative intensities of several bands could be observed. The vibrational mode most enhanced is the C−N stretching vibration around 1370 cm^{-1}. Other vibrational modes, including the bands at 1198, 1178, 491 (see Scheme 1), and 409 cm^{-1}, which highly involve the C−N stretching and CCN deformation motion, are

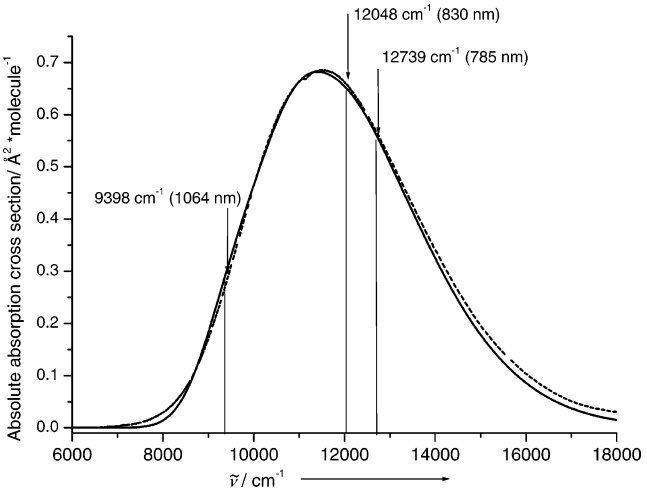

Figure 7. Absorption cross section of $\mathbf{1}^+$ (dashed line) and the calculated spectrum (solid line). The excitation lines used in the resonance Raman measurements are marked.

also significantly enhanced (Table 3). The symmetrical C═C stretching modes around 1600 cm^{-1} are also enhanced under resonant excitation conditions. Additionally, a vibrational mode at 1310 cm^{-1}, which was assigned to an *asymmetric* C−N stretching mode (Table 3, calculated at 1295 cm^{-1}), can be observed in the resonance Raman spectra, although it cannot be found in the off-resonance Raman spectrum. Nevertheless, the assignment of this band is disputable since the DFT calculations predicted a medium strong symmetric C−N stretch vibration at 1305 cm^{-1}, which is, however, similar to the mode most enhanced under resonant excitation predicted at 1337 cm^{-1} (a_g symmetry). So far, we can conclude that the charge-transfer excited-state potential surface is displaced along the above-mentioned normal mode coordinates.

Both the absorption spectra and resonance Raman spectra contain information about the excited-state potentials. The time-dependent treatment[31−33] of electronic and vibrational spectroscopy quantifies the absorption and resonance Raman cross sections, and thus, the quantitative analysis of the absorption and resonance Raman spectra allows the dimensionless displacement parameters Δ to be determined. The displacements are a measure of how far along a particular normal mode the molecule in one electronic state has to move in order to reach the geometry of the excited electronic state.[40] Generally, these are illustrated in one-dimensional representations of the potential energy surfaces along a normal mode where the distance between the minima of the parabolas is Δ.

The absorption and resonance Raman cross sections are given within the time-dependent theory[31−33] as a full Fourier transform and a half Fourier transform of the Franck−Condon factor, respectively. Due to the fact that this treatment is described extensively in the literature,[27,82−85] little detail will be given here.[86] Mode-specific information about the vibrational modes involved in the electronic transition can be obtained by simultaneously modeling both the resonance Raman intensity profiles and the absorption spectrum. Knowing the vibrational characteristics (from theoretical vibrational analysis; see Table 1) and the dimensionless displacement parameters Δ of the resonance enhanced vibrational modes, the latter can be converted into absolute bond distortions.[87−90] However, these depend on the sign of Δ, while the vibrational reorganization energies can be calculated directly from Δs and the corresponding wavenumbers.

Raman cross sections for the most RR enhanced vibrational modes (see Table 3) were determined by integrating over the respective bands and calculating the ratio of this value and the area of the CH_2Cl_2 band at 702 cm^{-1} of known cross section[87,91] which was used as an internal standard. Band deconvolution was performed where necessary. Correction for self-absorption was made as described in the literature.[41,92]

Following the general computational strategy described by Myers,[27,93] we simulated the absorption and differential Raman cross sections of the 10 symmetrical RR enhanced modes marked in bold in Table 3. The mode of very low intensity at 1310 cm^{-1}, which is most likely an asymmetrical N−Ar−N stretching vibration, has not been considered for the calculations since we lack the machinery to treat asymmetrical modes. The theoretical absorption and Raman cross sections for the symmetrical modes were calculated using the same input parameters. Harmonic ground- and excited-state potentials with equal force constants were considered. Within the Condon approximation, the derivatives of the transition dipole moment with respect to the vibrational coordinates were set to zero. We assumed a temperature of 298 K and no thermal population of higher vibrational levels of the electronic ground state. The electronic zero−zero energy as defined in Figure 1 for a symmetrical mode, E_{00}, which was estimated from the absorption spectrum and slightly modified during the fitting procedure, amounts to 8300 cm^{-1}. A small amount of static inhomogeneous broadening (250 cm^{-1}) corresponding to the zero−zero energy shifts had to be included, to suppress any vibrational feature in the absorption spectrum.

The solvent-induced broadening was taken into account in terms of a single overdamped Brownian oscillator model[94,95] and no damping due to the lifetime decay has been taken into account. The solvent induced "homogeneous" broadening[96] Γ_0 amounts to 1180 cm^{-1}, which corresponds[87,95] to a classical reorganization energy of $\lambda_s = 628$ cm^{-1}. The displacement

(82) Myers, A. B. *Chem. Rev.* **1996**, *96*, 911−926.
(83) Myers, A. B. *Annu. Rev. Phys. Chem.* **1998**, *49*, 267−295.
(84) Kelley, A. M. *J. Phys. Chem. A* **1999**, *103*, 6891−6903.
(85) Zink, J. I.; Shin, K. S. K. *Adv. Photochem.* **1991**, *16*, 119−214.

(86) The absorption cross section within the time-dependent formalism at wavenumber ω is given by:

$$\sigma_A(\omega) = 4\pi(eM)^2\omega/3\hbar c \int_{-\infty}^{\infty} d\delta G(\delta) \sum_i B_i \mathrm{Re} \int_0^{\infty} dt\langle\chi_i|\chi_i(t)\rangle \exp[i(\omega - E_{00} - \delta + \omega_i)t - g(t)]$$

where M is the transition moment, δ is some inhomogeneous distribution of zero−zero energy (E_{00}) shifts, B_i is the Boltzmann population of vibrational level i of energy ω_i, and $g(t)$ is a damping function due to the solvent induced broadening.

(87) Moran, A. M.; Kelley, A. M. *J. Chem. Phys.* **2001**, *115*, 912−924.
(88) Egolf, D. S.; Waterland, M. R.; Kelley, A. M. *J. Phys. Chem. B* **2000**, *104*, 10727−10737.
(89) Lilichenko, M.; Tittelbach-Helmrich, D.; Verhoeven, J. W.; Gould, I. R.; Myers, A. B. *J. Chem. Phys.* **1998**, *109*, 10958−10969.
(90) Baranovski, V. I.; Lubimova, O. O.; Makarov, A. A.; Sizova, O. V. *Chem. Phys. Lett.* **2002**, *361*, 196−202.
(91) Trulson, M. O.; Mathies, R. A. *J. Chem. Phys.* **1986**, *84*, 2068−2074.
(92) Shriver, D. F.; Dunn, J. B. R. *Appl. Spectrosc.* **1974**, *28*, 319−323.
(93) FORTRAN code for calculating absolute cross sections was obtained courtesy of Prof. Anne Myers Kelley at the University of California.
(94) Li, B.; Johnson, A. E.; Mukamel, S.; Myers, A. B. *J. Am. Chem. Soc.* **1994**, *116*, 11039−11047.
(95) Mukamel, S. In *Oxford Series in Optical and Imaging Sciences*; Lapp, M., Nishizawa, J.-I., Snavely, B. J., Stark, H., Tam, A. C., Wilson, T., Eds.; Oxford University Press: New York, 1995; Vol. 6, pp 209−261.

parameters for the RR-enhanced symmetrical modes are summarized in Table 3. The calculated vibrational reorganization energies for these vibrational modes are also listed.

Figure 7 shows that an excellent fit for the charge resonance absorption band shape could be obtained. The resonance Raman excitation profiles are included in the Supporting Information. Several points concerning the resonance Raman data are worth noting (see Table 3): A recent resonance Raman study of an organic mixed-valence system performed by Williams et al.,[42] based on the same procedure as the one applied in the study presented here, reported very good simulations for both the absorption and the relative Raman cross sections. However, the absolute Raman scattering cross sections were roughly an order of magnitude higher than those measured experimentally. The calculations were done on the diabatic surfaces of a symmetrical, localized charge-transfer system. To gain insight into the underlying Raman cross section problem, Williams et al.[42] approximated the upper and lower adiabatic surfaces with inequivalent, vertically displaced parabolic surfaces. However, under these conditions they found that the upper state frequencies were three times larger than the ground-state frequencies, which independent of other considerations leads to smaller calculated Raman cross sections. Adjusting all the parameters to such a harmonic potential energy diagram model, Williams et al. obtained Raman cross sections close to the experimental data. However, the absorption spectrum still could not be modeled exactly. The study of Williams et al.[42] showed rather convincingly that the discrepancies between the theoretical analysis and the experimental data lies in the unique shapes of the surfaces of a localized IV-CT system. In contrast, for a delocalized system ($\mathbf{1}^+$), a very good fit for both absorption and Raman cross sections could be obtained by modeling the ground- and excited-state potential surfaces with equivalent harmonic surfaces.

High displacement parameters were obtained for the vibrational modes in the low wavenumber region. The twisting of the phenyl groups at 257 cm^{-1} and the CNC deformation at 491 cm^{-1} which involves the axial C−N bonds have the highest distortion. However, the displacement of the symmetric C−N stretching along the bridge (Scheme 1) is also bigger than one. This mode at 1365 cm^{-1} has the largest displacement of all the stretching modes. The vibrational reorganization energies are proportional to the vibrational wavenumbers. Therefore, the reorganization energy involved in the symmetric C−N stretching mode is found to be the largest. The sum of the reorganization energies of all symmetrical vibrations that we were able to observe is about 2850 cm^{-1}.

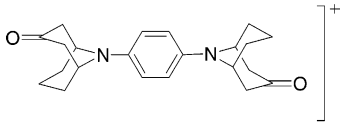

$\mathbf{2}^+$

These results can be compared with those recently obtained by Bailey et al. for the strongly coupled *p*-phenylenediamine $\mathbf{2}^+$ radical cation derivative.[22] In contrast to $\mathbf{1}^+$, the radical cation $\mathbf{2}^+$ shows an absorption band with strong vibrational progression. For system $\mathbf{2}^+$ the C═C stretch motion coupled with N−Ar−N stretching at 1620 cm^{-1} has the largest vibrational reorganization energy (see Table 3). In our system the symmetric C═C stretching is split into two modes at 1613 and 1582 cm^{-1}. The sum of the vibrational reorganization energies of these two modes is ca. 390 cm^{-1}, which corresponds to the 335 cm^{-1} value obtained in this vibrational region by Bailey et al.[22] for the corresponding mode. Much in contrast, the C−N stretching mode at 1365 cm^{-1} along the bridge shows the largest displacement and the largest contribution to λ_v in $\mathbf{1}^+$ but has much less intensity in the *p*-phenylenediamine derivative $\mathbf{2}^+$ probably due to substituent effects. The minimal total vibrational reorganization energy for $\mathbf{1}^+$ is, however, a factor of 2 larger than for the *p*-phenylenediamine derivative reported by Bailey et al.

Our fit of the resonance Raman and the absorption cross sections yields $\lambda_v \approx 2850$ cm^{-1} and $\lambda_s \approx 630$ cm^{-1}, which are the total vibrational reorganization energy and the solvent reorganization[95] energy, respectively. The sum of these reorganization energies (= 3480 cm^{-1}) compares very well with the reorganization energy $L = 4080$ cm^{-1} of the symmetric mode obtained from the Marcus−Hush theory (see section B and Figure 1). Together with E_{00} (= 8300 cm^{-1}) the sum of λ_v and λ_s (= 11 780 cm^{-1}) agrees very well with the optical transition energy ($\tilde{\nu}_{max} = 11\,580$ cm^{-1}):

$$\tilde{\nu}_{max} = E_{00} + \lambda_v + \lambda_s \qquad (10)$$

Furthermore, the solvent reorganization energy obtained from the analysis of the observed resonance Raman intensities is quite small. The obtained value of $\lambda_s \approx 630$ cm^{-1} is an upper limit and is more properly labeled as the classical reorganization energy since it may contain contributions from low-wavenumber vibrational modes that were not observed in the resonance Raman spectra. Such a mode at 205 cm^{-1} due to the out-of-plane deformation of the phenylene ring could be noticed in the spectrum recorded at 1064 nm. Barbara et al.[35] determined from resonance Raman data the classical reorganization energy for localized inorganic mixed-valence compounds in deuterated glycerol and water. The results of Barbara et al.[35,97] showed that the solvent-induced broadening of the absorption band is significant if the dipole moment of the solute changes upon optical excitation. The classical reorganization energy for localized MV systems obtained from RR data was in the range of 3300−3700 cm^{-1}, which is considerably higher than the value obtained for $\mathbf{1}^+$. The small contribution of the solvent to the reorganization energy and its small influence on the charge-transfer process is again a strong evidence for a delocalized system.

A theoretical analysis of Talaga and Zink about the effects of bond length changes and electronic coupling on the intensities

(96) The solvent induced broadening was taken into account in terms of a single overdamped Brownian oscillator model. This model appropriately describes both the solvent effects on the solute and the effect of the solute on the solvent. The time scale of the solvent induced breadth is usually expressed by the parameter $\kappa = \Lambda/D$. Here Λ determines the characteristic solvent time scale and D represents the strength of the coupling between the electronic transition and the solvation coordinate. We assumed slow modulation where $\kappa = 0.1$, which makes the solvent contribution to the absorption line shape nearly Gaussian. Thus, the function $g(t)$ becomes $g(t) = (D^2/\Lambda^2)\,[\exp(-\Lambda t/\hbar) - 1 + \Lambda t/\hbar)] + i(D^2/2k_BT)t/\hbar$ where the quantity $D^2/2k_BT$ represents the solvent contribution λ_s to the reorganization energy. Mukamel and co-workers showed that the solvent reorganization energy and solvent induced broadening are accounted for by the "homogeneous" broadening Γ_0: $D = \Gamma_0[(1 + 0.85\,\kappa + 0.88\,\kappa^2)/(2.355 + 1.76\,\kappa)]$.

(97) Kambhampati, P.; Son, D. H.; Kee, T. W.; Barbara, P. F. *J. Phys. Chem. A* **2000**, *104*, 10 637−10 644.

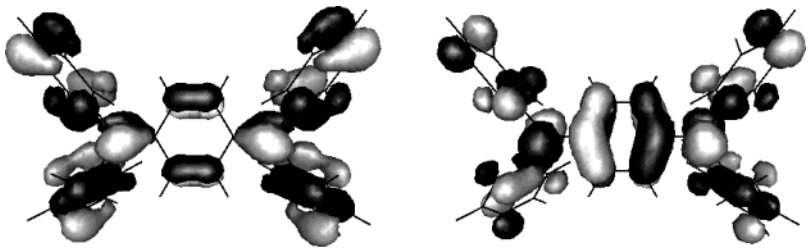

Figure 8. Contour plot of the molecular orbitals HOMO-1 and SOMO of $\mathbf{1}^+$ and their symmetries for a centrosymmetric molecular structure

of the symmetric and asymmetric modes in absorption and resonance Raman[29] spectra has shown that the symmetric mode intensity increases with increasing Δ_{coup} which is equivalent to the linear coupling constant l_y of the averaged symmetrical mode mentioned above. This parameter is a measure of the change in coupling as the molecule vibrates along the symmetric coordinate. Starting from a coordinate-displaced model for the potentials of interacting electronic states for a localized system, Talaga and Zink showed that as the sites move close together, the coupling increases. Talaga and Zink concluded that when the coupling (Δ_{coup}) is even larger in the direction of increasing valence delocalization, the symmetric modes become the most intense and their contribution to the spectra is more important. This behavior has also been found in the study of Bailey et al.[22] for a strongly delocalized system $\mathbf{2}^+$.

Within the framework of a dynamic vibronic model[24] developed by Coropceanu et al. to describe the CT electronic spectra, it could be shown that the diagonal coupling elements of the vibronic Hamiltonian lead to displacements of the ground vs excited state adiabatic potentials along symmetric modes. The effect of symmetric vibrational modes on the absorption band shape of delocalized mixed-valence systems was also recognized previously by Hush,[69,70] Piepho,[67] Schatz et al.,[8,68] and Ondrechen.[98,99] In the strong coupling limit, the absorption line shape is *controlled* by the symmetric modes. Our resonance Raman data in connection with the crystal structure analysis and DFT calculations for $\mathbf{1}^+$ are in agreement with the prediction made by Hush[69] that in general more than one symmetric vibration is involved into the electronic transition and that the primary symmetric mode was that formed by coupling the donor−bridge and bridge−acceptor stretch modes. Such a mode provides an apparent vibration in the donor−acceptor separation and was identified as the symmetric C−N stretch at 1365 cm^{-1} in the case of $\mathbf{1}^+$ (Scheme 1). Nevertheless, for $\mathbf{1}^+$ several symmetric vibrational modes are involved in the CT transition. This can probably be explained by an additional coupling of the monosubstituted benzene rings to the electronic transition. Therefore, a closer examination of the molecular orbitals of $\mathbf{1}^+$ is important to understand the charge-transfer process and the vibrational modes involved. Theoretical calculations performed by Coropceaunu et al.[100] within the framework of a single configuration interaction for *N*,*N*,*N*′,*N*′-tetrakis(4-methoxyphenyl)phenylenediamine showed that the CT transition is dominated by a HOMO-1 → SOMO one electron excitation. In the case of $\mathbf{1}^+$, the HOMO-1→ SOMO transition involves an excitation of an electron from a CN bonding to an antibonding orbital (see Figure 8), leading to a lengthening of the CN bond caused by the N−Ar−N stretch vibration observed around 1370 cm^{-1}. The fact that this vibrational mode presents a very high displacement parameter indicates a significant geometrical change of this bond in the excited state. Furthermore, the orbital coefficients of the phenyl units are larger in the HOMO-1 orbital than in the SOMO orbital. This indicates that vibrational modes involving the phenyl units are also coupled to the electronic transition.

The high number of vibrational modes involved into the charge resonance transfer makes it difficult to determine the effective bond length changes.[27,85,87] However, taking into account the considerations given above, the sign of the displacement parameters, which result in the lengthening or the shortening of the bonds, can be deduced. The mode at 1365 cm^{-1} induce alone a lengthening of 0.038 Å of the axial N−C bonds.

The difficulty in converting the dimensionless displacement parameters in bond length and angle changes consists, however, not only in their signs but also in selecting the vibrational mode coordinates. In the case of the C═C stretch, five sets of calculated coordinates could be taken into consideration for the two experimental Raman bands. Nevertheless, similar bond changes were obtained if the 1593 or 1595 cm^{-1} vibrations were considered for the 1582 cm^{-1} band. Thus, the calculation of the bond changes led to a lengthening of the axial N−C bonds by 0.05 Å, a shortening of the C1−C2 bonds by 0.018 Å, and a lengthening of the C2−C3 bonds by 0.015 Å. A significant change of the N−C7 bonds has been determined (0.021 Å). Changes of the phenyl ring bonds of less than 0.01 Å are predicted upon optical excitation.

Conclusions

The resonance Raman experiments showed that at least eight vibrational modes are strongly coupled to the optical charge resonance band. With the help of a DFT-based vibrational analysis, these modes were assigned mainly to symmetric vibrations. The resonance Raman intensity analysis allowed us to obtain mode-specific information about the excited-state potential energy surface even if the direct electronic absorption spectrum of $\mathbf{1}^+$ is completely diffuse. The vibrational reorganization energies for symmetrical modes were also quantified and the bond length changes upon optical excitation have been evaluated. The contribution of the symmetric vibrational modes to the reorganization energy is dominant. These findings are in agreement with the conclusions from the simple two-state two-mode Marcus−Hush analysis. In particular, quantitative agreement between the reorganization energy of the symmetric modes was obtained from both analyses. However, in contrast to the

(98) Root, L. J.; Ondrechen, M. J. *Chem. Phys. Lett.* **1982**, *93*, 421−424.
(99) Ko, J.; Ondrechen, M. J. *J. Am. Chem. Soc.* **1985**, *107*, 6161−6167.
(100) Coropceanu, V.; Malagoli, M.; Andre, J. M.; Bredas, J. L. *J. Chem. Phys.* **2001**, *115*, 10 409−10 416.

analysis of the resonance Raman data the asymmetric mode is also essential for a proper description of the absorption spectrum within the Marcus−Hush model. Nevertheless, according to this semiclassical analysis the ET barrier is tiny. Within the different restrictions of the two models (vibrational vs semiclassical) the conclusions about $\mathbf{1}^+$ are essentially the same. The excellent agreement of the X-ray crystal structure analysis and the DFT-computed molecular structure of $\mathbf{1}^+$ on one hand as well as the solvent and solid-state IR spectra and the DFT calculated IR active vibrations on the other hand prove $\mathbf{1}^+$ to adopt a symmetrical delocalized class III structure both in the solid state and in solution. Despite close structural resemblance of $\mathbf{1}^+$ and of $\mathbf{2}^+$ their absorption spectra are quite different; while $\mathbf{1}^+$ shows a broad asymmetric band that of $\mathbf{2}^+$ displays a distinct vibrational progression. This difference can be traced back to a different degree of mode contribution to the absorption spectra.

Acknowledgment. We thank the Fonds der Chemischen Industrie, the Deutsche Forschungsgemeinschaft (Graduiertenkolleg 690 "Elektronendichte"), JASCO GmbH Deutschland, and Dr. V. Coropceanu/Georgia Institute of Technology for preliminary DFT calculations and helpful discussions. The authors are most grateful to Prof. Dr. W. Kiefer for the technical and the financial support and for helpful scientific discussion as well as the use of the Raman laboratories. We thank Prof. Dr. Anne Myers Kelley and co-workers for providing the Fortran code to perform the resonance Raman analysis.

Supporting Information Available: Details of the crystal structure determination of **1**, $\mathbf{1}^+SbCl_6^-(THF)_{0.5}$, and $\mathbf{1}^+SbCl_6^-(dioxane)_{0.5}$ (cif) and details of the UV/vis/NIR, IR, and Raman measurement and the RR excitation profiles. This material is available free of charge via the Internet at http://pubs.acs.org. Crystallographic data (excluding structure factors) for the structures reported in this paper have been deposited with the Cambridge Crystallographic Data Centre as supplementary publication no. CCDC-221196, 221197, and 221510. Copies of the data can be obtained free of charge on application to CCDC, 12 Union Road, Cambridge CB2 1EZ, UK [fax: (internat.) + 44(1223)336-033; e-mail: deposit@ccdc. cam.ac.uk].

JA0395386